Supporting Information

Electrolyte additive strategy for uniform nucleation of Cu-Bi toward low-voltage self-powered dynamic windows

Xi Wang [a],Yiming Bai [a,b,*], Fei Han [a], Yichen Jiao [a], Yuzhe Guan [a], Jinjing Bai [a], Fuzhi Wang [a], Meicheng Li [a], Guicheng Liu [a,c,d,*]

[a] State Key Laboratory of Alternate Electrical Power System with Renewable Energy Sources, North China Electric Power University, Beijing 102206, China

[b] Key Laboratory of Semiconductor Materials Science, Beijing Key Laboratory of Low Dimensional Semiconductor Materials and Devices, Institute of Semiconductors, Chinese Academy of Sciences, Beijing 100083, China

[c] Fujian Provincial Key Laboratory of Eco-Industrial Green Technology, Wuyi University, Wuyishan, Fujian Province, 354300, China

[d] Key Laboratory of Power Station Energy Transfer Conversion and System of Ministry of Education and School of Energy Power and Mechanical Engineering, and Beijing Laboratory of New Energy Storage Technology, North China Electric Power University, Beijing, 102206, China

*Corresponding authors' E-mail addresses:

ymbai@ncepu.edu.cn (Yiming Bai), gcliu@ncepu.edu.cn, log67@163.com (Guicheng Liu)

Experimental Section

Materials:

Bismuth chloride ($BiCl_3$, 99.99%), Copric chloride dihydrate ($CuCl_2 \cdot 2H_2O$, 99.99%), Lithium chloride (LiCl, 99%), Choline chloride (ChCl, 99%), Ethylene glycol (EG, 99%), Lead(II) acetate trihydrate ($Pb(Ac)_2 \cdot 3H_2O$, 99.5%), L-Phenylalanine (L-PAA, 99.99%), Poly(vinyl alcohol) and bis(trifluoromethane) sulfonimide lithium salt (LiTFSI, 99%) were purchased from Innochem Technology Co., Ltd. (Beijing, China). Cesium iodide (CsI, 99.9%), lead (II) iodide (PbI_2, 99.9%), lead(II) bromide ($PbBr_2$, 99.9%) and Spiro-OMeTAD (99.8%)were purchased from Xi'an Yuri Solar Co., Ltd. (Xi'an, China). Tin oxide (IV) (15% in H_2O colloid dispersing solution), dimethyl sulfone (DMSO, 99.7%+), ultra-dry chlorobenzene (CB, 99%), acetonitrile (anhydrous, 99.8%), 4-tert-butylpyridine (TBP, 98%), ethanol (99.5%) and molybdenum trioxide (MoO_3) were purchased from Alfa Aesar (Shanghai, China). Hydrochloric acid (HCl, 35-36%) was purchased from Shanghai Suitry Chemical Technology Co., LTD. N, N'-Dimethylformamide (DMF, 99.8%) was purchased from Aladdin.

Material and device characterization:

The cyclic voltammetry (CV), electrochemical impedance spectroscopy (EIS), chronoamperometry (CA), and Johnson-Mehl-Avrami-Kolmogorov (JMAK) analysis were performed on electrochemical workstation (ModuLab XM ECS) using a standard three-electrode system (Tianjin Aida Hengsheng Technology Development Co., Ltd.). Ag/AgCl and Pt electrodes were used as the reference electrode and counter electrode, with bare ITO as the working electrode. All EIS data were normalized by the surface area of the working electrode to enable direct comparison with literature values. The transmittance and absorption spectra of the UV-Vis spectrum were measured by UV–vis NIR3600 spectrometer (Shimadzu, Japan). Current density–voltage (*J*–*V*) curves of solar cells were measured by a solar simulator (San-Ei Electric Co., Ltd., Class AAA grade, AM1.5G solar irradiation with a light intensity of 100 mW cm^{-2}) with a Keithley 2400 digital source controlled by computer. The standard Si solar cell purchased from the National Renewable Energy Laboratory was utilized to calibrate light intensity. External quantum efficiency (EQE) curves were measured by the QE-R system of Enli Technology under ambient atmosphere. The scanning electron microscope (SEM) and energy-dispersive X-ray spectroscopy (EDX) characterization were scanned by HITACHI Model SU8600 field emission scanning electron microscope (FE-SEM). The ultraviolet photoelectron spectroscopy (UPS) was measured by the Thermo ESCALAB 250XI ultraviolet photoelectron spectrometer equipped with a monochrome ultraviolet light source ($h\nu$ = 21.22 eV).

JMAK analysis:

Crystal growth geometry factor and crystal nucleation frequency during cycling were evaluated by JMAK analysis. The analysis was performed using $X=1-\exp(-kt^n)$, where X represents the reaction ratio, t is the reaction time, n is the crystal growth geometry factor, and k is the crystal nucleation frequency. Each cycle of the JMAK test includes 0 V for 2 s and -1 V for 10 s. The current-time (*I-t*) curves were extracted every 200 cycles, for a total of 2000 cycles. During the process of the cycle, 0 V for 2 s and -1.0 V for 10 s was applied for the metal film formation for every cycle. The parameters n and k were estimated from the intercept and slope and were consolidated into Figure 2e, f, following the analysis of $\ln[-\ln(1-X)] = \ln k + n \ln t$.

Computational methods:

All binding energy calculations based on density functional theory (DFT) were performed in the DMol3 module project. The generalized gradient approximation (GGA) with the PerdewBurke-Ernzerhof (PBE) functional was employed to describe the exchange-correlation energy.

The simulation uses the physical field interface of tertiary current distribution in the electrochemical module of COMSOL Multiphysics software to simulate two electrode surfaces. This model was based on the calculation of current in the electrolyte and electrode using the "tertiary current distribution" interface.

The surfaces of electrodes are simulated by using the physical field interface of tertiary current distribution in the electrochemical module of COMSOL Multiphysics software. This model was based on the calculation of current in the electrolyte and electrode with the "tertiary current distribution" interface. The electrolyte current was solved according to Ohm's law. One electrode was grounded, and the other electrode was set to the battery potential to satisfy the total current condition. In the simulation, expressions in the form of Butler-Volmer were used to describe the electrode kinetics that occur on the electrode surface, and it is assumed that the exchange current density of the redox reaction is related to the concentration. The current density on the electrode surface was represented by the Butler-Volmer equation:

$$i_a = i_0\left(\frac{c}{c_0}\exp\left(\frac{\eta(1-\beta)F}{RT}\right) - exp(\frac{\eta\beta F}{RT}\right) \#(S1)$$

where i_a, i_0, c, c_0, η, β, F, R, and T represent the current density, exchange current density, ion concentration on the electrode surface, bulk ion concentration, overpotential, charge transfer coefficient, Faraday constant, gas constant, and thermodynamic temperature, respectively. The definition of overpotential is as follows:

$$\eta = \Phi_s - \Phi_l - E_{eq} \#(S2)$$

where Φ_s, Φ_l, and E_{eq} represent electrode potential, electrolyte potential, and equilibrium potential, respectively. The transport of dissolved ions in the electrolytes generated by the electrode reaction was simulated through a transient simulation of the "dilute species transport" interface, which

assumed that the transport of ions can be described by diffusion according to Fick's law.

Formula calculation and related parameter description:

$$|j_p| = 0.446c\sqrt{\frac{F^3n^3Dv}{RT}}\#(S3)$$

$$\kappa = \frac{F^2}{RT}\sum Z_i^2 D_i C_i\#(S4)$$

In Equation S3, j_P is the peak current density (A cm^{-2}), c is the concentration of redox-active species (mol cm^{-3}), F is the Faraday constant (C mol^{-1}), n is the number of electrons transferred during oxidation-reduction process, D is the diffusion coefficient (cm^2 s^{-1}), v is the scan rate (V s^{-1}), R is the gas constant (J mol^{-1} K^{-1}), and T is the absolute temperature (K). In Equation S4, the ionic conductivity κ of the electrolyte solution can be represented as the sum of contributions from each ion, where Z_i, C_i, and D_i are the charge, concentration, and diffusion coefficient corresponding of ion i.

For the equivalent circuit in Figure 4d and Figure S5f, a pure resistance and a pseudo capacitor element were connected in parallel to describe a semicircle in the Nyquist plot. Here, the equivalent circuit consists of three equivalent circuit elements: R_s represents the resistance of the electrode and electrolyte, R_{ct} is the charge transfer resistance, the constant phase angle element (CPE) is applied to represent the capacitive effect, which is defined by two parameters (CPE-T and CPE-P). The value of CPE-P generally ranges from 0 to 1, and 1 means the electronic component is a pure capacitor and 0 represents a resistor.

$$I_p = 2.65 \times 10^5 \times n^{3/2} \times A \times D^{1/2} \times C \times v^{1/2}\#(S5)$$

The diffusion coefficients of Cu^{2+} and Bi^{3+} during the reduction process can be obtained based on Equation S5, where I_p represents the peak current, n is the number of electrons transferred during the oxidation-reduction process, A is the electrode area, D is the diffusion coefficient, C represents the metal ion concentration, and v is the scan rate.

The transmittance fluctuation factor (T_{ff}) within a certain wavelength range is an important parameter for measuring the color rendering performance of RMED, and the T_{ff} is definition by Equation S6:

$$T_{ff} = (\frac{1}{N}\sum_{i=1}^{N}(T_i - T_{avg})^2)^{1/2}\#(S6)$$

where N is the number of wavelengths, T_i is the transmittance value at a specific wavelength, and T_{avg} is the average transmittance within the measured wavelength range.

The conductivities (σ) of SnO_2 and SnO_2/L-PAA films were measured with a structure of ITO/ETL/Au, which can be calculated by Equation S7,

$I = \sigma A d^{-1} V \#(S7)$

where A is the device area, d is the thickness of ETL, I and V are current and voltage.

As shown in Figure S6g, the lowest unoccupied molecular orbital (LUMO) level of SnO_2/L-PAA (-4.23 eV) offers a favorable energy level matching with $Pb(Ac)_2$-$CsPbI_2Br$ (-4.17 eV), ensuring the photovoltage output of $CsPbI_2Br$ solar cells. The highest occupied molecular orbital (HOMO) level of SnO_2/L-PAA (-7.99 eV) also provides a better hole-blocking ability, leading to higher V_{oc}.

For the equivalent circuit in Figure 5e, R_s is the series resistance including the interface layer, active layer, and wire resistance. R_t and R_{rec} are the charge transfer resistance and recombination resistance, while C_t and C_{rec} are the chemical capacitances representing the transfer and recombination processes.

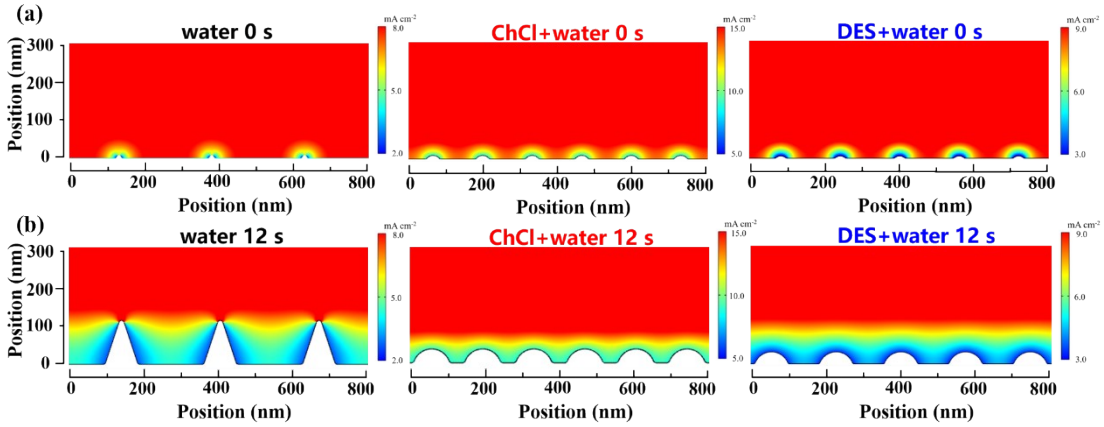

Figure S1. COMSOL simulation of current density distribution at -0.6 V for (a) 0 s and (b) 12 s in water, ChCl+water, and DES+water solvent systems.

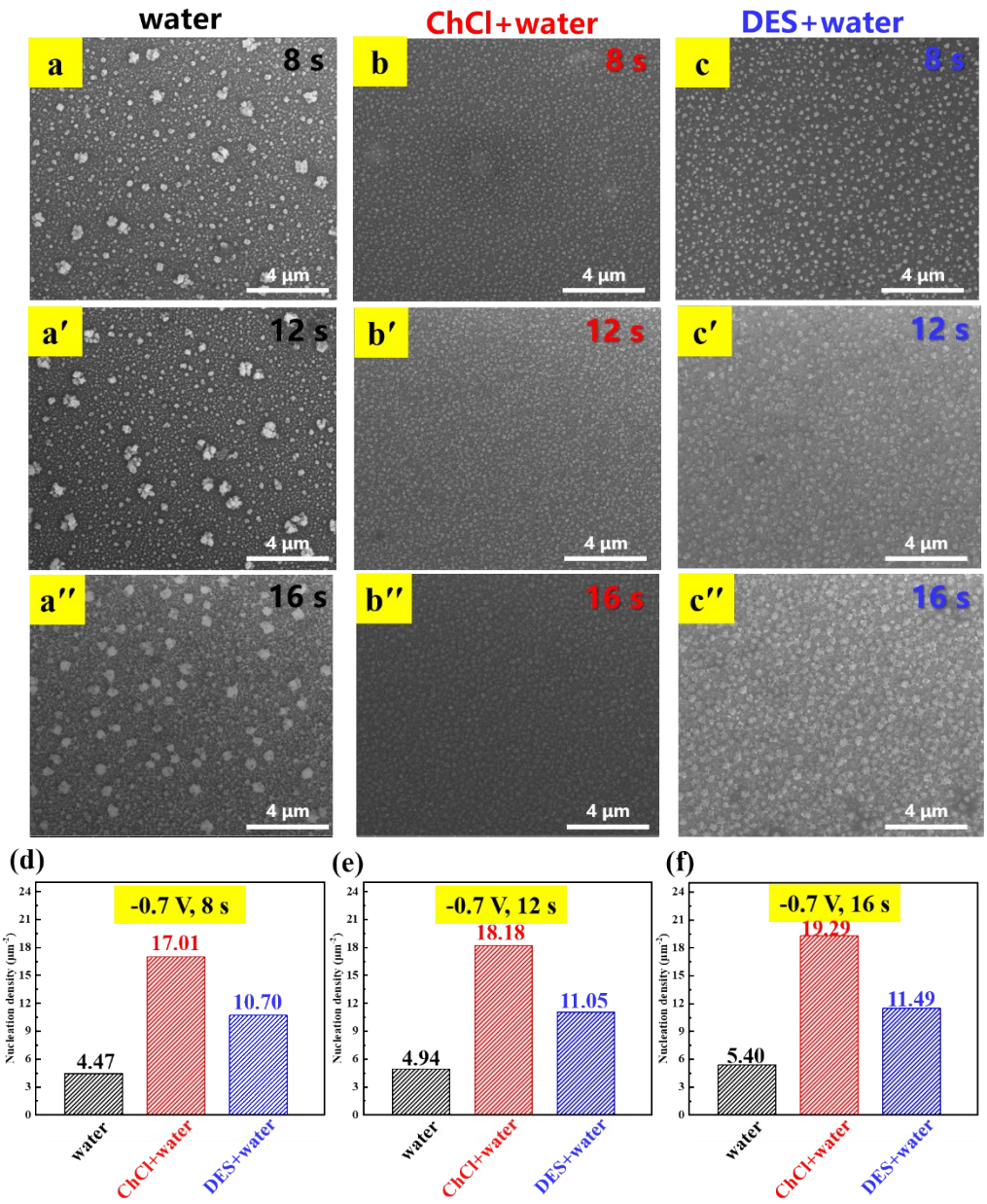

Figure S2. The SEM images of electrodeposition in the water electrolyte under -0.70 V for 8 s (a), 12 s (a′), and 16 s (a″), ChCl+water electrolyte under -0.70 V for 8 s (b), 12 s (b′), and 16 s (b″), DES+water electrolyte under -0.70 V for 8 s (c), 12 s (c′), and 16 s (c″). The corresponding nucleation densities of three electrolytes under deposition time of 8 s (d), 12 s (e), and 16 s (f).

Table S1. The nucleation densities, average particle sizes, and surface coverage ratios at -0.70 V for 8, 12, and 16 s.

Deposition conditions	evaluation parameter	water	ChCl+water	DES+water
-0.70 V, 8 s	nucleation density (μm^{-2})	4.47	17.01	10.70
	average particle size (nm)	73.24	62.07	72.25
	surface coverage ratio (%)	26.60	34.08	28.35
-0.70 V, 12 s	nucleation density (μm^{-2})	4.94	18.18	11.05
	average particle size (nm)	76.00	74.62	77.79
	surface coverage ratio (%)	31.29	38.36	32.23
-0.70 V, 16 s	nucleation density (μm^{-2})	5.40	19.29	11.49
	average particle size (nm)	81.06	81.74	83.24
	surface coverage ratio (%)	35.70	44.83	36.32

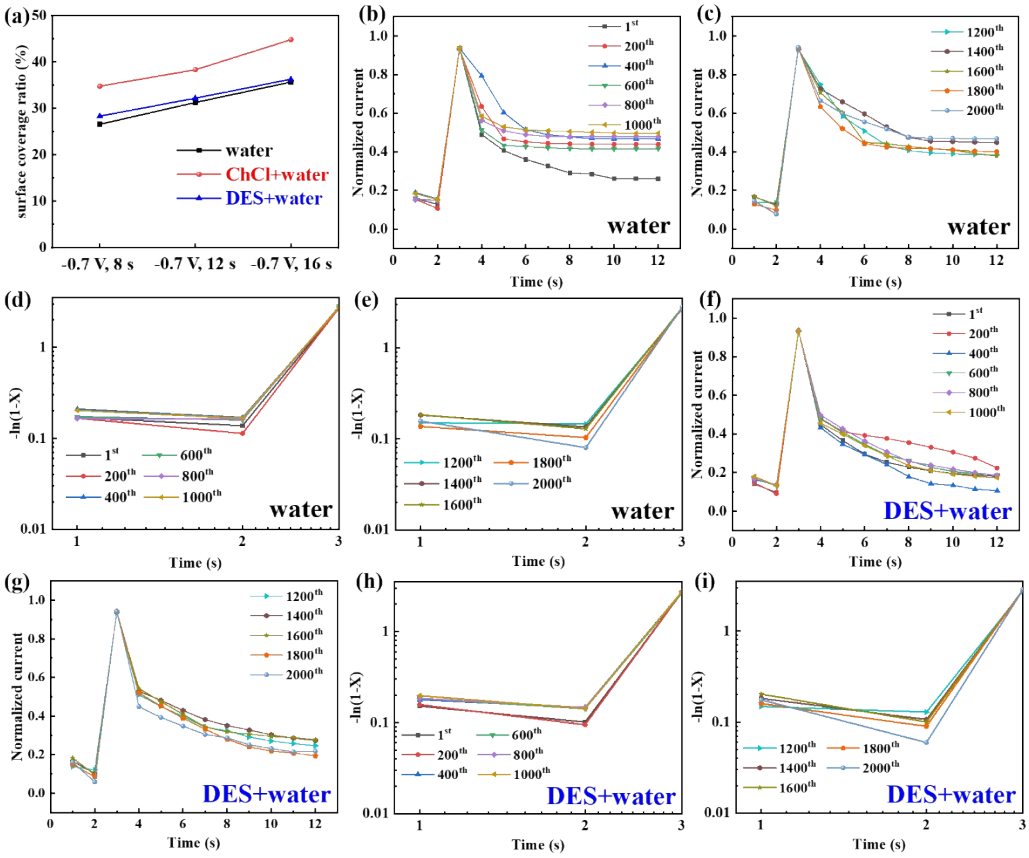

Figure S3. (a) The surface coverage ratio of three electrolytes when deposited at -0.7 V for 8, 12, and 16 s. The JMAK analysis of electrodeposition in (b~e) water electrolyte and (f~i) DES+water electrolyte.

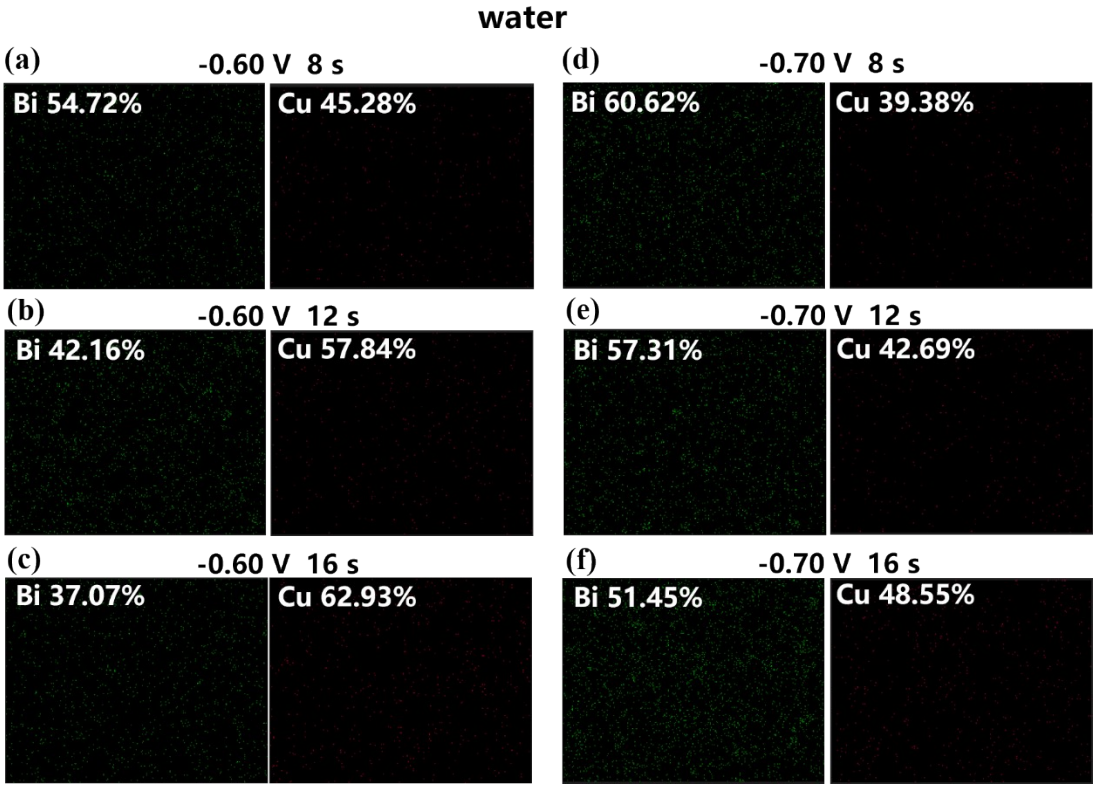

Figure S4. The EDX diagrams of Bi and Cu elements for water electrolyte at deposition conditions of (a) -0.60 V for 8 s, (b) -0.60 V for 12 s, (c) -0.60 V for 16 s, (d) -0.70 V for 8 s, (e) -0.70 V for 12 s, and (f) -0.70 V for 16 s.

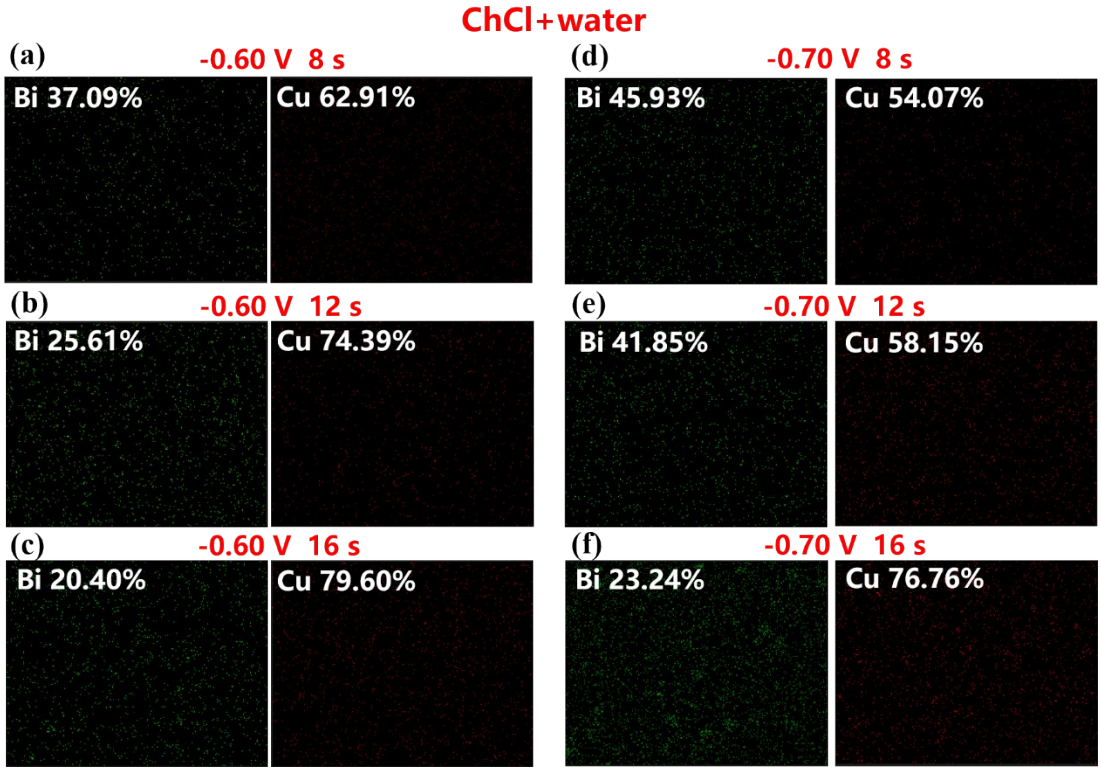

Figure S5. The EDX diagrams of Bi and Cu elements for ChCl+water electrolyte at deposition conditions of (a) -0.60 V for 8 s, (b) -0.60 V for 12 s, (c) -0.60 V for 16 s, (d) -0.70 V for 8 s, (e) -0.70 V for 12 s, and (f) -0.70 V for 16 s.

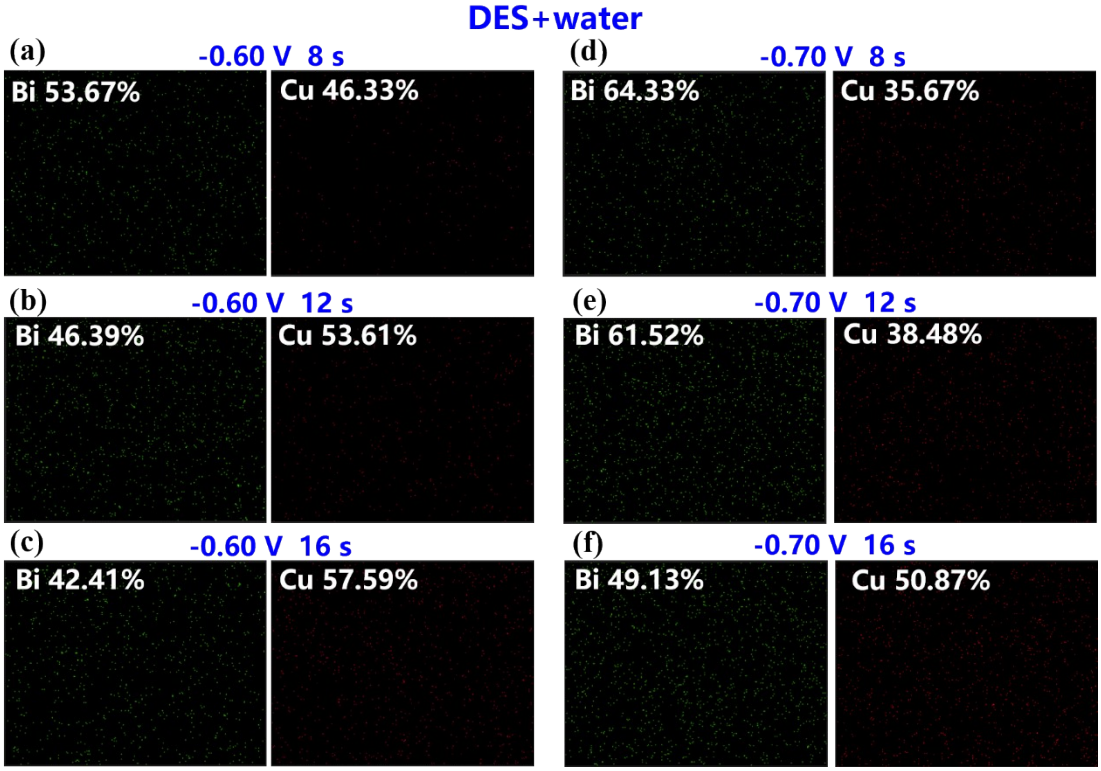

Figure S6. The EDX diagrams of Bi and Cu elements for DES+water electrolyte at deposition conditions of (a) -0.60 V for 8 s, (b) -0.60 V for 12 s, (c) -0.60 V for 16 s, (d) -0.70 V for 8 s, (e) -0.70 V for 12 s, and (f) -0.70 V for 16 s.

Table S2. Atom ratios of Cu and Bi under different deposition conditions.

At%	water -0.60 V, 8 s	ChCl+water -0.60 V, 8 s	DES+water -0.60 V, 8 s	water -0.70 V, 8 s	ChCl+water -0.70 V, 8 s	DES+water -0.70 V, 8 s
Cu	45.28	62.91	46.33	39.38	54.07	35.67
Bi	54.72	37.09	53.67	60.62	45.93	64.33
At%	water -0.60 V, 12 s	ChCl+water -0.60 V, 12 s	DES+water -0.60 V, 12 s	water -0.70 V, 12 s	ChCl+water -0.70 V, 12 s	DES+water -0.70 V, 12 s
Cu	57.84	74.39	53.61	42.69	58.15	38.48
Bi	42.16	25.61	46.39	57.31	41.85	61.52
At%	water -0.60 V, 16 s	ChCl+water -0.60 V, 16 s	DES+water -0.60 V, 16 s	water -0.70 V, 16 s	ChCl+water -0.70 V, 16 s	DES+water -0.70 V, 16 s
Cu	62.93	79.60	57.59	48.55	76.76	50.87
Bi	37.07	20.40	42.41	51.45	23.24	49.13

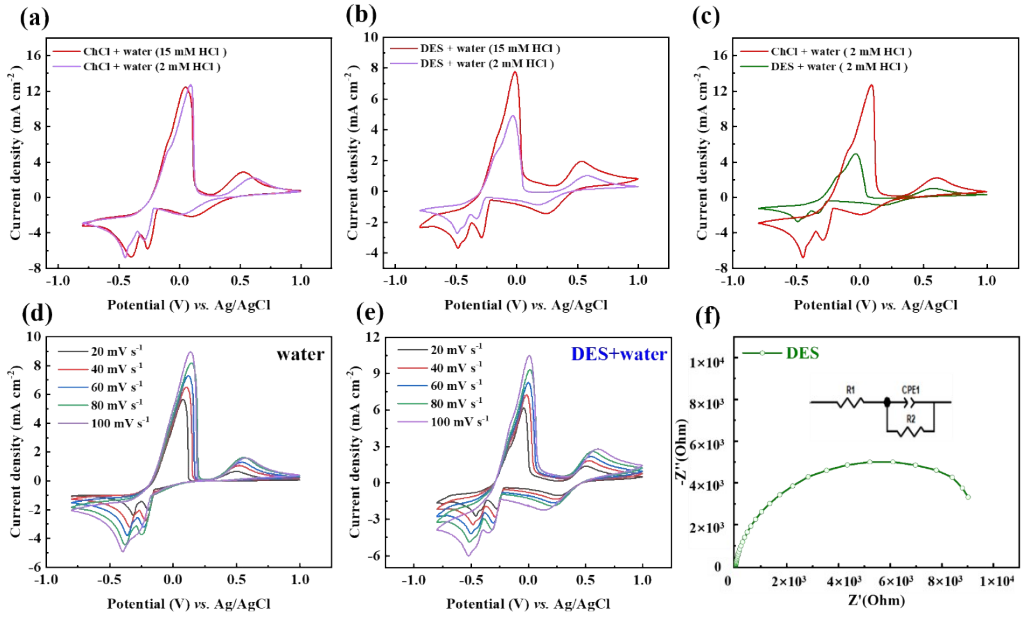

Figure S7. CV curves of (a) ChCl+water and (b) DES+water electrolytes containing 15 mM and 2 mM concentrations of hydrochloric acid. (c) CV curves of ChCl+water and DES+water electrolytes with 2 mM HCl. CV curves of (d) water and (e) DES+water electrolytes at different scan rates. (f) The electrochemical impedance Nyquist plots of DES electrolyte.

Table S3. The T_{ff} of devices based on different electrolytes at bias voltages of -0.58 and -0.60 V.

Bias voltage (V)	water	ChCl+water	DES+water
-0.58	2.0356	1.5046	2.1304
-0.60	2.0761	1.9791	2.0081

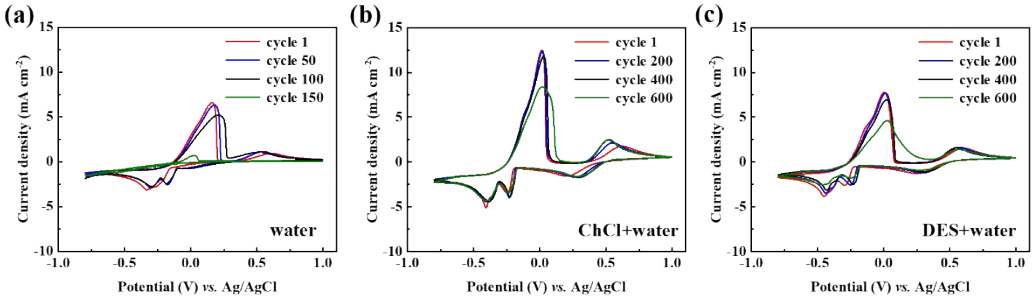

Figure S8. Multiple CV curves of (a) water, (b) ChCl+water, and (c) DES+water electrolytes.

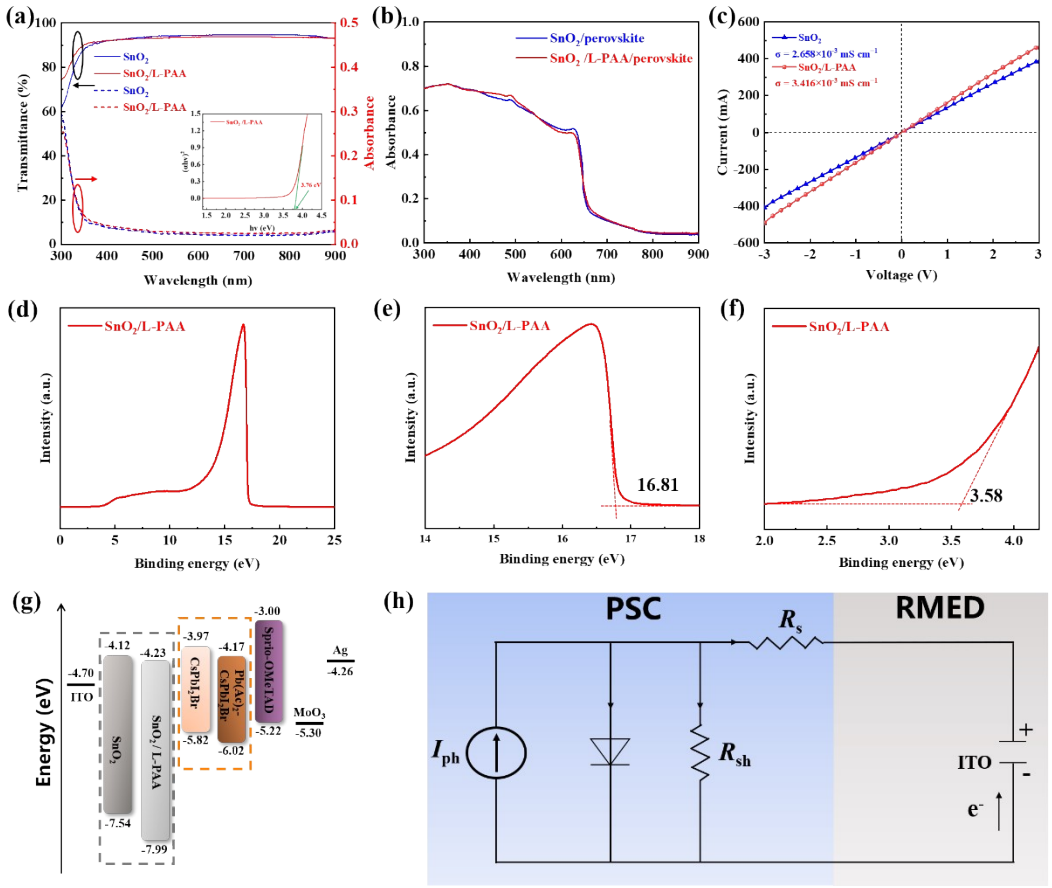

Figure S9. (a) The transmittance of SnO_2 and SnO_2/L-PAA films. (b) UV-vis absorption spectra of perovskite deposited on SnO_2 and SnO_2/L-PAA. (c) Conductivity of SnO_2 and SnO_2/L-PAA films. (d) UPS spectra of SnO_2/L-PAA film. UPS spectra in the (e) cutoff and the (f) onset region for the SnO_2/L-PAA film. (g) The energy level structure of the solar cells. (h) Equivalent circuit diagram of the RMED-SC.

Table S4. The EIS fitting parameters of solar cells

Samples	R_s ($\Omega \cdot cm^2$)	R_t ($\Omega \cdot cm^2$)	C_t (F)	R_{rec} ($\Omega \cdot cm^2$)	C_{rec} (F)
$CsPbI_2Br$	60.12	809.51	5.71×10^{-6}	2921	5.54×10^{-9}
$Pb(Ac)_2$-$CsPbI_2Br$	57.05	686.27	3.02×10^{-6}	3770	3.24×10^{-9}
L-PAA /$Pb(Ac)_2$-$CsPbI_2Br$	49.24	309.14	1.77×10^{-6}	4690	3.12×10^{-9}